frontiers | Frontiers in Earth Science

TYPE Original Research
PUBLISHED 11 July 2025
DOI 10.3389/feart.2025.1513583

OPEN ACCESS

EDITED BY
Li Tian,
China University of Geosciences
Wuhan, China

REVIEWED BY
Magdalena Matusiak-Malek,
University of Wrocław, Poland
Debajyoti Paul,
Indian Institute of Technology Kanpur, India

*CORRESPONDENCE
Saijun Sun,
sunsaijun06@163.com
Junjie Zhang,
zhangjunjie@qdio.ac.cn
Wei Guo,
gw02108106@126.com

RECEIVED 18 October 2024
ACCEPTED 24 June 2025
PUBLISHED 11 July 2025

CITATION
Cheng M, Sun S, Lou Y, Min Y, Tang Y, Li X, Zhang M, Hu X, Wan T, Zou H, Xu K, Chen C, Zhang J and Guo W (2025) Geochronology and geochemistry of mafic igneous rocks in the Zhegu area of southern Tibet.
Front. Earth Sci. 13:1513583.
doi: 10.3389/feart.2025.1513583

Geochronology and geochemistry of mafic igneous rocks in the Zhegu area of southern Tibet

Ming Cheng[1], Saijun Sun[2,3]*, Yuanlin Lou[1,4,5], Yingzi Min[1], Yao Tang[1], Xinyue Li[1], Ming Zhang[1], Xuming Hu[1], Tianyong Wan[1], Hao Zou[1], Kaihong Xu[1], Chao Chen[6], Junjie Zhang[2,3]* and Wei Guo[1]*

[1]Changsha Natural Resources Comprehensive Survey Center, China Geological Survey, Changsha, China, [2]Laboratory for Marine Geology, Qingdao Marine Science and Technology Center, Qingdao, China, [3]Center of Deep Sea Research, Institute of Oceanology, Chinese Academy of Sciences, Qingdao, China, [4]Institute of Mineral Resources, Chinese Academy of Geological Sciences, Beijing, China, [5]China University of Geosciences, Beijing, China, [6]Kunming General Survey of Natural Resources Center, China Geological Survey, Changsha, China

The Zhegu region, located in southern Tibet, is positioned within the central and eastern segments of the Tethys Himalayan tectonic belt. In this area, mafic igneous rocks are predominantly intrusion into Jurassic strata, occurring as vein-like bodies. This study presents zircon U-Pb age determinations and whole-rock geochemical analyses of diabase and gabbro samples from the region, aimed at elucidating their petrogenesis and geodynamic background. The zircon U-Pb ages yield crystallization ages of 130.7 ± 1.5 Ma for diabase and 131.6 ± 2.5 Ma for gabbro, both of which are consistent with the crystallization ages of ocean island basalt (OIB)-type mafic rocks in the Comei Large Igneous Province (130–136 Ma). Geochemical data reveal that these mafic rocks are characterized by elevated TiO_2, FeO^T, and P_2O_5 contents, alongside relatively low MgO content, indicative of tholeiitic affinities. They exhibit enrichment in light rare earth elements (LREEs) and high field strength elements (HFSEs) such as Nb, Hf and Y, resembling OIB signatures. These rocks show evidence of fractional crystallization without significant crustal contamination. Melting models suggest that the magmas originated from partial melting of a garnet-lherzolite mantle source. The petrogenetic characteristics of these rocks reflect interactions between the Kerguelen mantle plume and the overlying lithospheric mantle.

KEYWORDS

zircon U-Pb age, whole-rock geochemistry, OIB-like type mafic rocks, Kerguelen mantle plume, southern Tibet

1 Introduction

The Qinghai-Tibet Plateau is the youngest, highest, and largest plateau on Earth. Its formation resulted from the closure of the New Tethys Ocean, following the collision between the Indian Plate and the Eurasian Plate. This tectonic event led to the development of the Himalayan orogenic belt, which serves as a natural laboratory for studying plate tectonics and the geological evolution of the Tethys region. Situated in the northern part of the Himalayan Mountain system, the Tethys Himalayan Belt extends along the northern

edge of the Indian subcontinent, marking the forefront of the Cenozoic collision orogeny between the Indian and Eurasian plates. The magmatic activity and tectonic evolution preceding this orogenic event, particularly during the Mesozoic, have garnered significant interest in recent years as they are key to understanding the boundary conditions and material processes involved in the Cenozoic orogeny of the Himalayan Mountain system (Yin, 2006; Zhu et al., 2009a; 2013; Huang et al., 2018; Yang et al., 2022; Yu and Liu, 2023).

Previous studies have identified extensive Early Cretaceous mafic igneous rock formations in the eastern region of the Tethys Himalayan belt, particularly in areas such as Comei, Cona, and Longzi. These formations primarily span two time intervals: 140–150 Ma and 130–136 Ma (Zhu et al., 2007, 2008a, b; Xia et al., 2012; Wang et al., 2016; Ding et al., 2020; Cheng et al., 2022). Based on their geochemical characteristics, these mafic rocks could be classified into three types: Ocean Island Basalt (OIB)-like, Normal Mid-Ocean Ridge Basalt (N-MORB)-like, and Enriched Mid-Ocean Ridge Basalt (E-MORB)-like. These rocks are believed to have formed in an extensional environment characterized by significant lithospheric stretching and thinning along the northern margin of the Gondwana continent (Zhu et al., 2008a; b; Xia et al., 2012; Wang et al., 2016; Ding et al., 2020; Cheng et al., 2022). The onset of this extensional environment is thought to be related to continental breakup driven by the Kerguelen mantle plume (e.g., Zhu et al., 2009b). These OIB-like, E-MORB-like and N-MORB like igneous rocks are collectively referred to as the Comei Large Igneous Province (LIP), which is hypothesized to represent the early-stage magmatism associated with the Kerguelen mantle plume (e.g., Zhu et al., 2013). There are at least three distinct episodes of Cretaceous mafic magmatism within the Comei LIP area, and only the magmatic event earlier than 120 Ma is considered to be directly linked to Kerguelen mantle plume activity (Wang et al., 2016, 2024). Consequently, distinguishing the igneous rocks associated with the Comei LIP is critical for advancing our understanding of the Kerguelen mantle plume.

Mafic to intermediate dykes are extensivein the Zhegu region, yet detailed investigations into their petrogenesis and potential links to Comei LIP remain lacking. In this study, we present zircon U-Pb dating and whole rock major and trace elements of mafic rocks in the Zhegu area to elucidate their formation age, petrogenesis and tectonic settings. Additionally, we compile data on Early Cretaceous magmatic rocks exhibiting OIB and N/E-MORB like affinities within the Comei LIP. These data provide critical constraints for understanding the relationship between mafic rocks in the Zhegu area and the Comei LIP.

2 Geological background and samples

The Himalayan tectonic belt is subdivided into four tectonic units, arranged from north to south: the Tethys Himalayan, the High Himalayan, the Low Himalayan, and the Sub-Himalayan (Figure 1b). The Tethys Himalayan lies between the Yarlung Zangbo Suture Zone (IYS) and the Southern Tibetan Detachment System (STDS) and is part of the northern section of Greater India in paleogeographic terms. It is regarded as the typical passive continental margin since the Late Triassic period along the northern margin of Greater India (Yu and Wang, 1990).

The study area is located in the eastern part of the Tethys Himalayan region and is classified within the Kangmar Lhunze stratigraphic zone of the Gangdise Himalayan stratigraphic region. These strata are primarily controlled by regional faults with a northwest-southeast orientation (Figure 1b). Exposed strata in study area predominantly comprise Mesozoic to Cenozoic sedimentary rocks, particularly those from the Triassic and Jurassic periods. This stratigraphic sequence begins with the Upper Triassic Nieru Formation (T_3n), characterized by gray-black, thin to medium-layered silty slate interbedded with gray, medium-layered feldspar quartz sandstone and fine sandstone. This is followed by the Lower to Middle Jurassic Ridang Formation (J_1r), which comprises gray, dark gray, and gray-black mudstone, siltstone, sandstone, and shale. The Lower to Middle Jurassic Lure Formation ($J_{1\text{-}2}l$) presents a lithological assemblage of gray mudstone and sandstone, mudstone and limestone, as well as interbedded mudstone and limestone. The sequence continues with the Middle Jurassic Zhela Formation (J_2z), primarily composed of mudstone sandstone and silty mudstone. The region is characterized by numerous thrust faults oriented nearly east-west and northwest-southeast, as well as extensional faults oriented nearly north-south. Magmatic activity in this area was intensive, with volcanic rocks, mainly basalts, occurring predominantly within the Jurassic strata. Intrusive rocks are also widespread, often as veins in strata of the Jurassic Lure and Zhela Formation, with lithologies including pyroxenite, gabbro, diabase, and diorite. Notably, gabbro and diabase are exposed within the Zhegu area of the Comei LIP (Figure 1c), and extending in an east-west direction for approximately 20 km in length and 0.5–2 km in width.

The gabbros in this study are gray-black, massive, and predominantly composed of plagioclase (~45%), clinopyroxene (~40%), biotite (~6%), amphibole (~4%) and quartz (~4%). Plagioclase occurs as subhedral columnar grains ranging from 0.2 to 1 mm in diameter, with some grains altered to sericite and clay minerals. Clinopyroxene exhibits a subhedral granular morphology, with grain sizes of 0.3–1 mm, and is partially altered to hornblende and chlorite. Biotite is platy, with lengths ranging from 0.3 to 1 mm. Hornblende is subhedral granular and irregular, with 0.3–1 mm in diameter. Quartz, is anhedral and ranges from 0.1 to 0.2 mm in size (Figures 2a,c,e).

The diabases are grayish-green, massive, and display an ophitic texture. They are primarily composed of plagioclase (~45%), clinopyroxene (~30%), biotite (~5%), amphibole (~3%), Fe-Ti oxide (~4%), and quartz (1%). Plagioclase occurs as euhedral columnar grains, 0.5–1.5 mm in diameter, and is significantly altered to sericite and clay minerals. Clinopyroxene appears as subhedral granular shape, with diameters of 0.3–1 mm. Biotite is euhedral and platy, measuring 0.5–1.1 mm in size. Amphibole is diamond-shaped morphology and is altered to chlorite. Quartz, which, fills voids within clinopyroxene and plagioclase, is anhedral and granular. Additionally, Fe-Ti oxides occur as anhedral granular grains (Figures 2b,d,f).

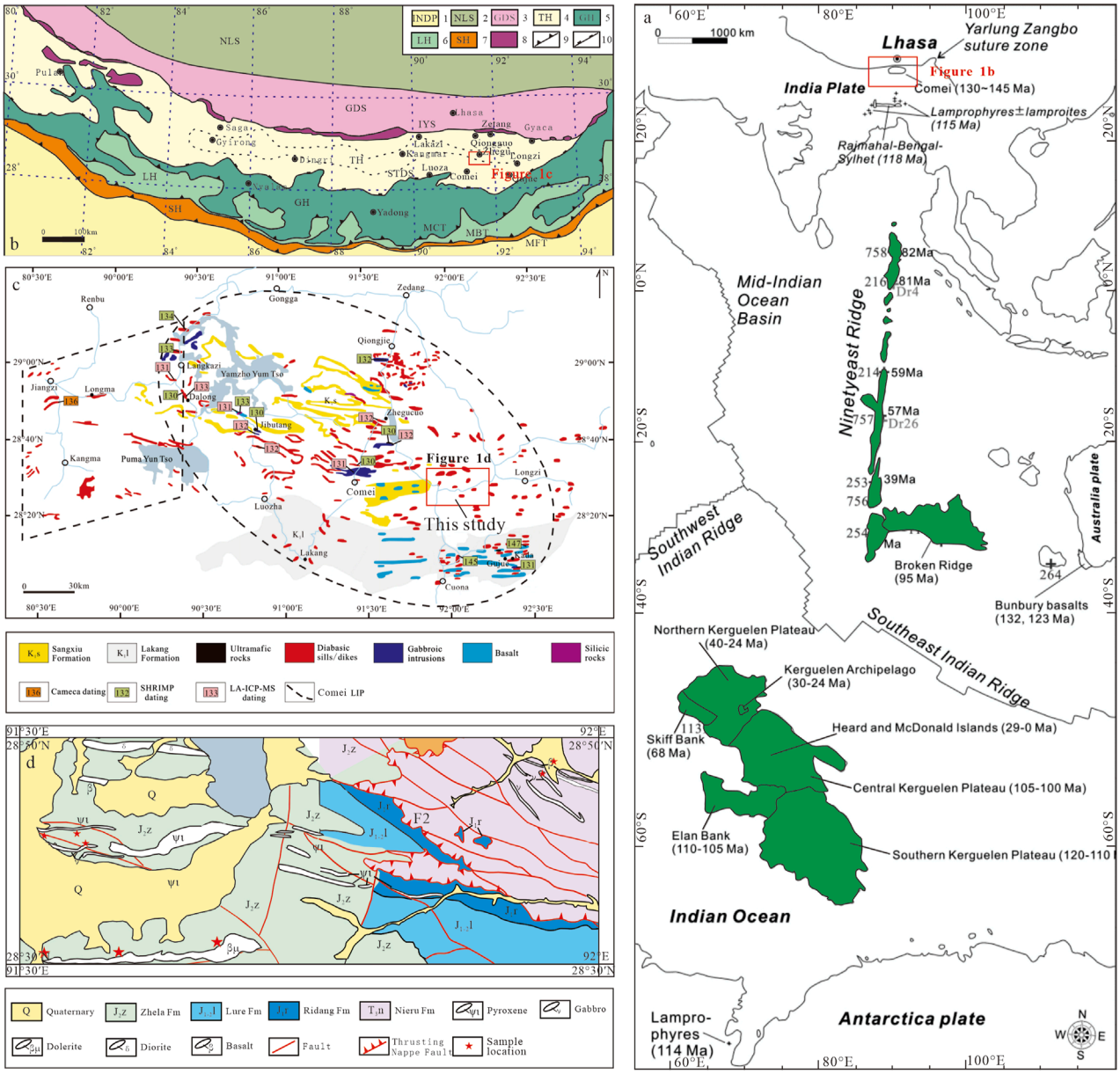

FIGURE 1
The Kerguelen hotspot-related basalt provinces in the Indian Ocean region **(a)** (after Coffin et al., 2002; Zhu et al., 2008b); Geotectonic map of southern Tibet **(b)** (after Liang et al. (2011)); Simplified geological map of the Comei large igneous province **(c)** (after Zhu et al. (2009a); Qiu et al. (2010)); **(d)** Geological map of the Zhegu area. 1-Indian plate; 2-Northern Lhasa Massif; 3-Gangdise island arc; 4-Tethys Himalaya; 5-High Himalayas; 6-Low Himalayan; 7-Sub-Himalayan; 8-Yarlung Tsangpo river ophiolite belt; 9-Thrust fault; 10-Slip fault; IYS-Yalung Zangbo suture; STDS-South Tibet detachment; MCT-Main central thrust; MBT-Main boundary thrust; MFT-Main front thrust. Location of samples in this study are in the Supplementary Table 1.

3 Analytical methods

The gabbro (sample numbers XML001, XML002, XML003, XML004) and diabase (sample numbers ZGL001, ZGL002) were collected for whole-rock major and trace elements analyses, and representative samples (ZGL001, XML001) were selected for zircon U-Pb dating.

Zircons were collected from whole-rock samples using the standard crushing, sieving, heavy liquid, and magnetic separation techniques, and selected under a binocular microscope. These zircons were mounted in an epoxy disk with the zircon standard SL13 from the Australian National University Research School of Earth Sciences and several TEM zircons for reference from the Australian Geological Survey. Subsequently, they were polished down to expose the interior texture. Cathodoluminescence (CL) imaging was obtained at the Institute of Mineral Resources, Chinese Academy of Geological Sciences, using an Oxford MINICL detector.

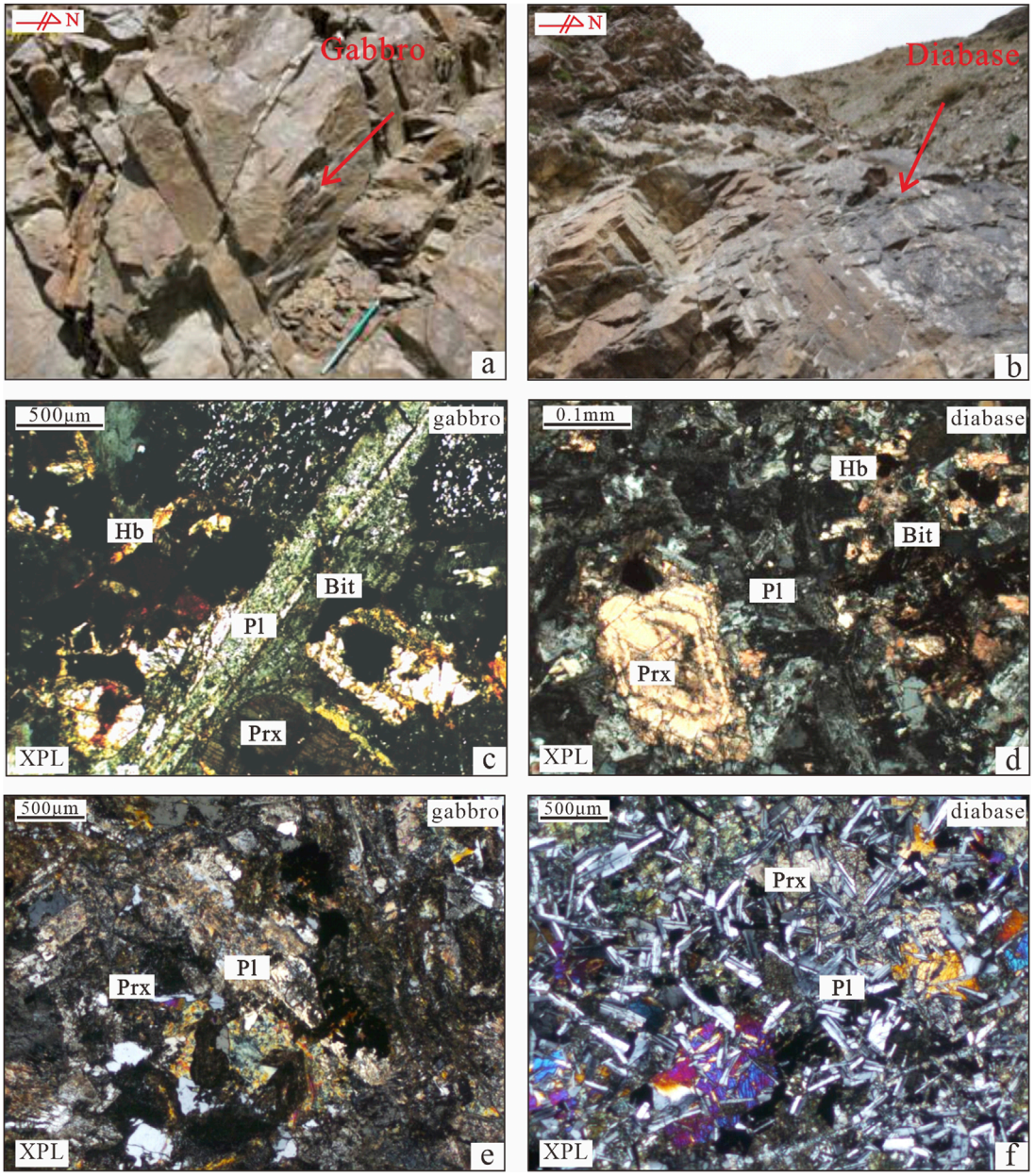

FIGURE 2
Field contacts **(a,b)** and Photomicrographs **(c–f)** of mafic dyke from the Zhegu area in southern Tibet. Pl, plagioclase; Prx, pyroxene; Hb, hornblende; Bit, Biotite.

SHRIMP zircon U-Pb analyses were conducted at the Beijing SHRIMP Center, using the standard zircon TEM (~417 Ma) for the calibration of instrumental mass fractionation. The U, Th, and Pb contents of the zircons were calibrated using the SL13 zircon, which has an age of ~572 Ma and a U content of 238 ppm. The instrument and its comprehensive operating principles were the same as previously described (Liu et al., 2003; Sun et al., 2018).

The compositions of major and trace elements were conducted at the Hunan Institute of Mineral Testing and Utilization. Major elements were analyzed by an atomic fluorescence spectrometer (AFS-830A, Jitian Instruments, Beijing, China) and atomic absorption spectrometer (Z-2300, Hitachi Limited, Tokyo, Japan). Trace elements were analyzed by ICP-OES (ICAP6300, Thermo Fisher Scientific, Waltham, MA, USA) and rare earth elements were analyzed by ICP-MS (Thermo X2, Thermo Fisher Scientific, Waltham, MA, USA). The analytical precision for major elements was better than 5%, and that of the rare earth and trace elements was better than 10% (Cheng et al., 2024).

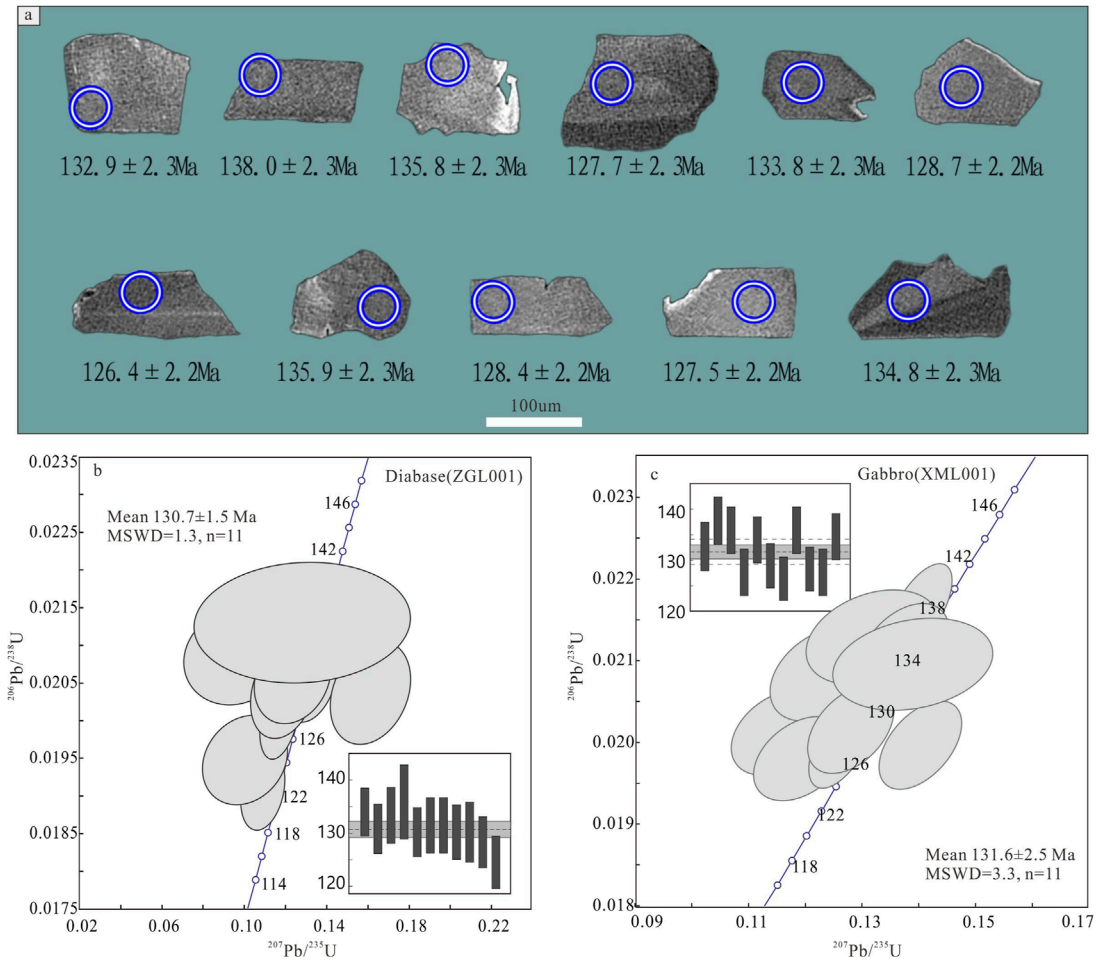

FIGURE 3
Zircon U-Pb cathodoluminescence images **(a)** and concordia diagrams **(b,c)** of mafic dyke rocks from the Zhegu area in southern Tibet.

4 Results

4.1 Zircon U-Pb ages

Supplementary Table 2 summarizes the U-Pb age data for mafic igneous rocks from the Zhegu area. The zircons are euhedral to subhedral, with lengths ranging from 110 to 180 μm and length/width ratios of 1:1 to 3:1 (Figure 3a). Cathodoluminescence (CL) imagings reveal that many zircons display characteristic oscillatory zoning (Figure 3a). The thorium (Th) and uranium (U) contents of the zircon samples vary significantly between different rock types. For the ZGL001 sample (diabase), Th and U contents range from 157 to 943 ppm and from 140 to 690 ppm, respectively. In contrast, the XML001 sample (gabbro) shows Th and U contents ranging from 578 to 5918 ppm and from 446 to 2052 ppm, respectively. The Th/U ratios of zircons, ranging from 1.16 to 2.19 in the diabase and from 1.30 to 2.98 in the gabbro, are consistently greater than 0.5 which is the characteristics of magmatic zircon (Hoskin and Black, 2000; Lin et al., 2019). Zircon U-Pb dating results for both diabase and gabbro indicate that all data points lie on or near the Concordia line (Figure 3). The calculated Concordia ages are 130.7 ± 1.5 Ma (MSDW = 1.3, Figure 3b) for the diabase and 131.6 ± 2.5 Ma (MSDW = 3.3, Figure 3c) for the gabbro.

4.2 Whole-rock major and trace elements

The contents of major and trace elements of mafic rocks from the Zhegu area of southern Tibet are presented in Supplementary Table 3.

4.2.1 Major elements

The mafic igneous rocks in the Zhegu area exhibit SiO_2 contents ranging from 50.2 to 52.6 wt.%, plotting within the basalt region on the TAS diagram (Figure 4a). These rocks are characterized by relatively high TiO_2 (2.83–4.98 wt.% with an average of 3.74 wt.%), FeO^T (9.07–11.6 wt.% with an average of 9.93 wt.%), and P_2O_5 content (0.47–1.22 wt.% with an average of 0.63 wt.%). The MgO content is relatively low, ranging from 3.32 to 5.39 wt.%. The $Mg^{\#}$ values, which range from 37.5 to 50.2, are significantly lower than those of primary basaltic magma ($Mg^{\#}$ = 68–75; Wilson, 1989). These rocks were plotted in the area of the tholeiitic series (Figure 4b). The aluminum

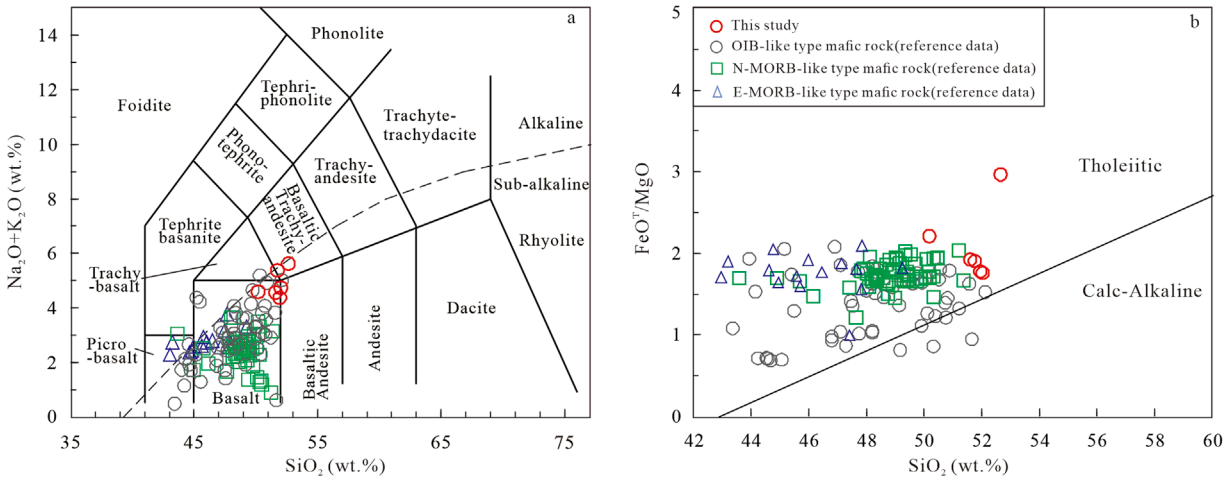

FIGURE 4
(a) SiO_2 versus K_2O + Na_2O [after Middlemost (1994)]; **(b)** FeO^T/MgO versus SiO_2 [modified from Miyashiro (1974)] diagrams of mafic dyke rocks from the Zhegu area. The mafic igneous rocks from nearby areas in previous studies, including OIB-like type, N-MORB-like type and E-MORB-like type, are also plotted for comparison. OIB-like type data are from Zhu et al. (2005), Zhu et al. (2007), Zhu et al. (2008b); N-MORB-like type data are from Zhu et al. (2008b), Wang et al. (2016), Wang et al. (2022), and Qiu et al. (2010), E-MORB-like type data from Jiang et al. (2007), Tong et al. (2007), Ding et al. (2020), and Yu and Liu (2023).

saturation indexs (A/CNK) range from 0.63 to 0.77. Additional geochemical parameters further characterize their composition: the Ritter index (σ) ranges from 1.92 to 2.96, the alkalinity rate (AR) ranges from 1.53 to 1.76, and the total alkali content (ALK) ranges from 4.38 to 5.64 wt.%. The consolidation index (SI) varies between 17.2 and 26.8, while the differentiation index (DI) spans from 41.8 to 53.8.

4.2.2 Trace elements

The mafic rocks from the Zhegu area in southern Tibet exhibit total rare earth element (REE) contents ranging from 225 to 296 ppm, with a notable enrichment in light rare earth elements (LREE) (LREE/HREE = 2.37–2.73). These rocks also show significant fractionation between LREE and heavy rare earth elements (HREE), with La/Yb ratios ranging from 6.09 to 8.20. The resulting right-skewed REE patterns closely resemble those of OIB (Figure 5a) (Sun and McDonough, 1989). Notably, there are no discernible anomalies in Eu and Ce. The trace element spider diagram reveals enrichment in Nb and Hf, coupled with a depletion of Y, and the distribution patterns closely resemble those of OIB (Figure 5b). The ratios of Ti/Y, Th/Ta, Th/Yb, Ce/Zr, and Zr/Y are 377–642, 0.64–1.75, 0.79–1.55, 0.21–0.31, and 5.53–9.30, respectively, aligning closely with those observed in OIB basalts (Supplementary Table 3; Pearce, 1982; Zhu et al., 2005).

5 Discussion

5.1 Formation ages

The crystallization ages of diabase and gabbro in this study are 130.7 ± 1.5 Ma and 131.6 ± 2.5 Ma, respectively. These crystallization ages are comparable to those of OIB-like igneous rocks in the southern and western regions of the Comei LIP, where the peak magmatic activity occurred ~132 Ma. Furthermore, these ages align with the early-stage magma activity associated with the Kerguelen mantle plume event (Zhu et al., 2009a; Ding et al., 2020). The close temporal coincidence suggests a genetic relationship between the mafic igneous rocks in the Zhegu area and early-stage magma activity of the Kerguelen mantle plume.

5.2 Petrogenesis

5.2.1 Crustal contamination

We propose that the mafic rocks in the Zhegu area have undergone limited crustal contamination. The La/Sm ratio is generally considered stable, but it could increase significantly (>5.00) during crustal contamination (Lassiter and DePaolo, 1997; Zhang et al., 2004). The La/Sm ratio of the Zhegu mafic rocks ranges from 2.94 to 3.38, and in the La/Sm vs. La/Nb diagram (Figure 6a), the samples do not exhibit a trend consistent with crustal contamination. Similarly, the Ce vs. Nb/Th diagram (Figure 6b) shows no linear trend, further indicating minimal crustal influence (Condie et al., 2002; Rudnick and Gao, 2003). In the $(Th/Ta)_{PM}$ vs. $(La/Nb)_{PM}$ diagram (Figure 6c), the Zhegu mafic rocks are distinctly separated from the upper, middle, and lower crust, resembling the characteristics of Hawaiian Island basalt, 90° E ridge basalt, and Kerguelen OIB. The $(La/Nb)_{PM}$ vs. $(Th/Nb)_{PM}$ diagram (shows that the samples in this study plot in the region of basalts unaffected by crustal contamination (Figure 6d; Neal et al., 2002). Additionally, crustally contaminated magma typically shows negative anomalies in Nb, Ta, and Ti (Thompson et al., 1984; Wilson, 1989), which are not apparent in the Zhegu mafic rocks. The Nb content in the upper, middle, and lower crust (12 ppm, 10 ppm, 5 ppm, respectively) is significantly lower than that in these mafic rocks (30.4–42.8 ppm), further suggesting minimal crustal contamination.

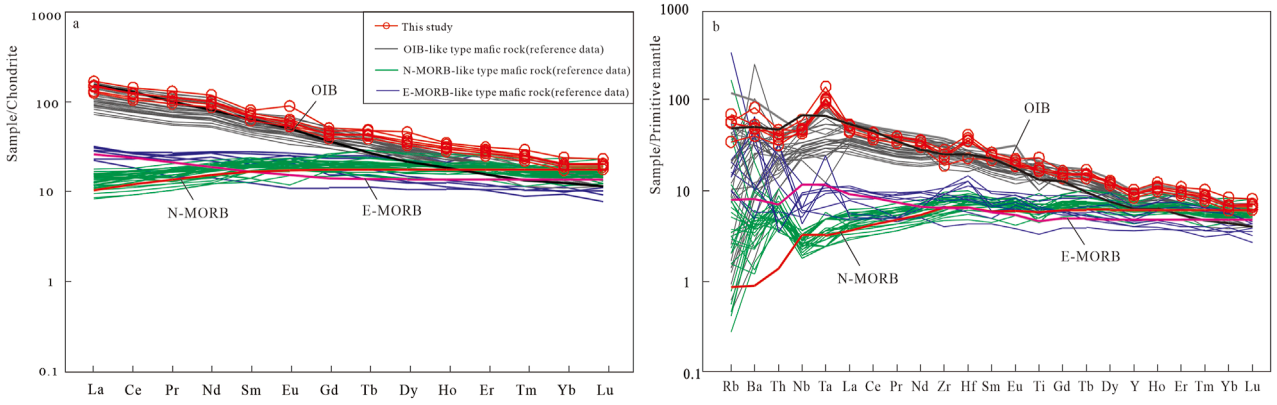

FIGURE 5
Chondrite-normalized REE patterns **(a)** and Primitive mantle-normalized trace elements spider diagrams **(b)** of mafic dyke from the Zhegu area in southern Tibet. Normalizing values are from Sun and McDonough (1989). Reference data are the same as those for Figure 4.

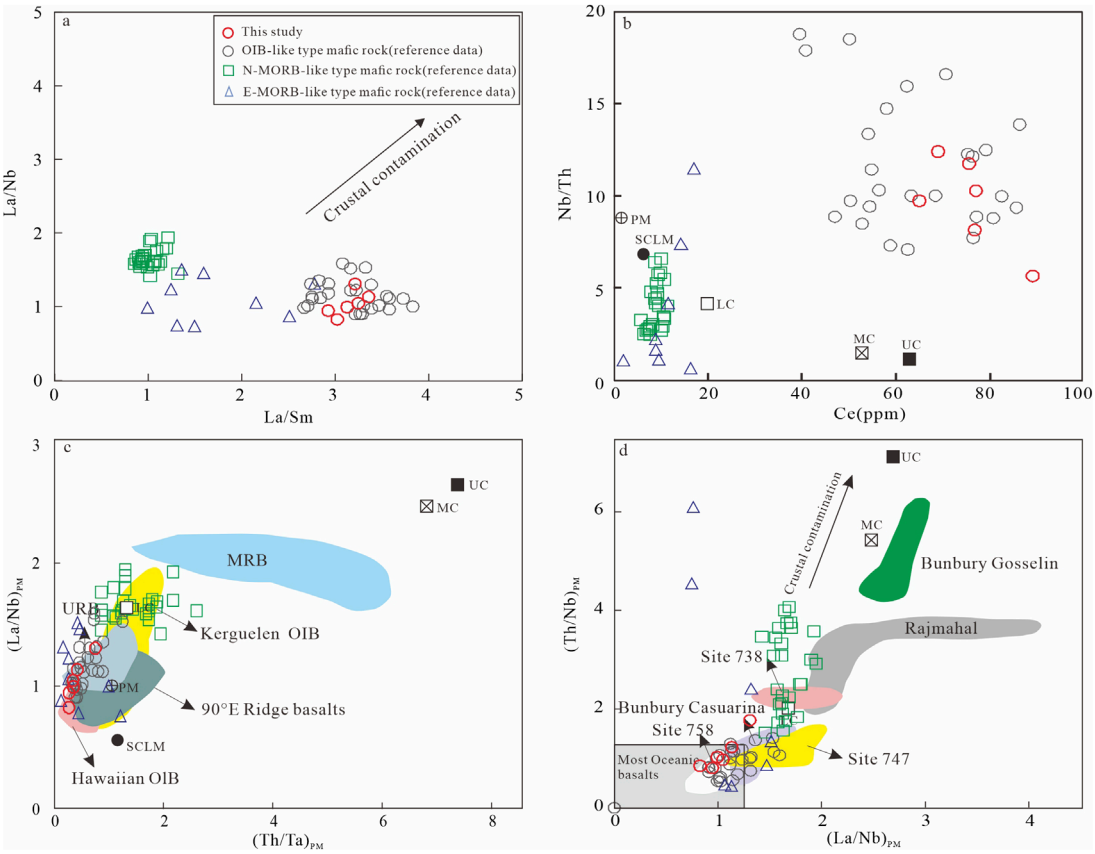

FIGURE 6
(a) The La/Sm versus La/Nb [after Zhu et al. (2007)]; **(b)** Ce versus Nb/Th [after Zhu et al. (2007)]; **(c)** $(Th/Ta)_{PM}$ versus $(La/Nb)_{PM}$ [after Zhu et al. (2005)]; **(d)** $(Th/Nb)_{PM}$-$(Nb/U)_{PM}$ [after Huang et al. (2018)] diagrams of mafic dyke rocks from the Zhegu area in southern Tibet. UC, MC and LC represent upper crust, middle crust and lower crust (Rudnick and Gao, 2003). PM: primitive mantle (Taylor and McLennan, 1985); SCLM: subcontinental lithosphere mantle (McDonough, 1990); URB and MRB: Rajmahal basalts not contaminated by the crust and contaminated by the crust; Bunbury Casuarina and Bunbury Gosselin basalts' data are from Frey et al. (1996); Data of Rajmahal dark rocks are from Baksi (1995) and Kent et al. (1997). Data of Site 747 basalts are from Frey et al. (2002); data of Site 738 basalts are from Mahoney et al. (1995); data of Site 758 basalts are from Neal et al. (2002). Other reference data are the same as those for Figure 4.

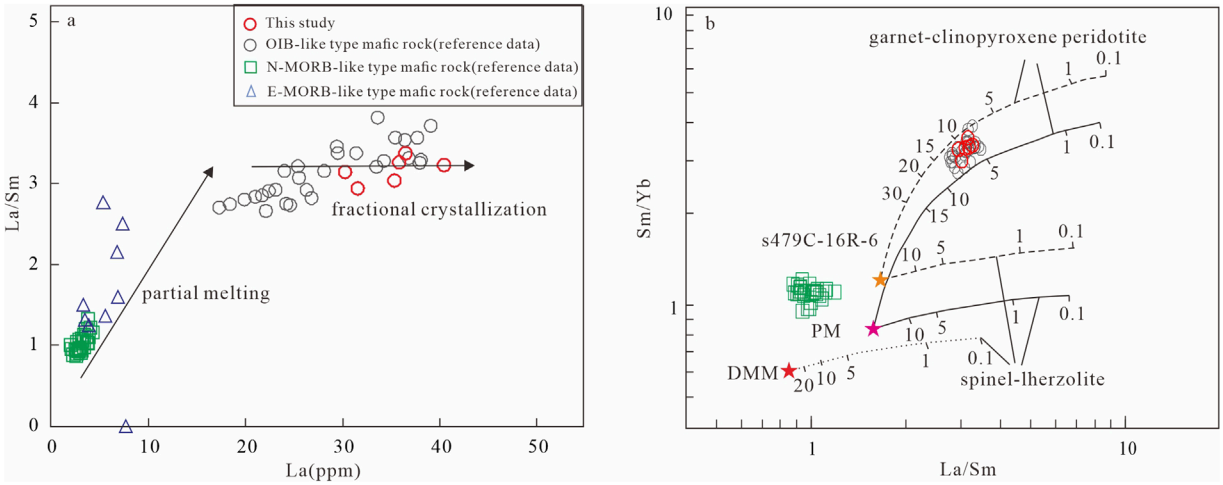

FIGURE 7
The La versus La/Sm **(a)** and La/Sm versus Sm/Yb **(b)** (Shaw, 1970) discrimination diagrams of the mafic dyke rocks from the Zhegu area in southern Tibet. Melt curves for spinel-lherzolite (with mineral mode of Ol.53%+Opx.27%+Cpx.17%+ Sp.3%; Kinzler, 1997) and garnet-clinopyroxene peridotite (with mineral mode of Ol.53.3%+ Cpx.35.7%+ Gt.11.0%, Walter, 1998) were drawn following the approach of Aldanmaz et al. (2000). Mineral/matrix partition coefficients are from McKenzie and O'Nions (1991); Depleted MORB Mantle (DMM) compositions are from Workman and Hart (2005); PM compositions are from Sun and McDonough (1989) and the sample s749C-16R-6 data are from Frey et al. (2000). The dashed curves represent the melting trend of sample s749C-16R-6 compositions; the solid and dot curves are the melting trends from PM and DMM, respectively. Tick marks on each curve correspond to degrees of partial melting (%) for a given mantle source.

Overall, the geochemical characters of the Zhegu mafic rocks strongly indicate that they have not been significantly contaminated by crustal material.

5.2.2 Magma mechanism

Partial melting and fractional crystallization are two primary mechanisms driving magmatism and its evolution. These processes can be differentiated using the La-La/Sm discriminant diagram (Figure 7a), where the samples exhibit a horizontal linear distribution, suggesting fractional crystallization as the dominant process.

Additionally, the $Mg^{\#}$ of the samples ranges from 37.5 to 50.2, which is significantly lower than the $Mg^{\#}$ of primary basaltic magma (68–75) (Wilson, 1989), indicating a high degree of magma differentiation. The concentrations of compatible elements, such as Ni and Cr, are notably low, ranging from 5.6 to 63.6 ppm and 8.0–100 ppm, respectively. The Harker diagrams show a positive correlation between $Mg^{\#}$ and Ni, Cr (Figures 8a,b), indicating the significant fractional crystallization of olivine and clinopyroxene (Frey et al., 1978; Hess, 1992). As $Mg^{\#}$ decreases, the CaO and Al_2O_3 contents either increase or remain stable (Figures 8f,h), with no evidence of a negative Eu anomaly in the REE patterns (Figure 5). It is worth noting that these mafic rocks contain significant amounts of plagioclase (Figure 2), suggesting that the plagioclase did not separate from the magma following its crystallization. Furthermore, the correlations between $Mg^{\#}$ and Zr and P_2O_5 are negative and not obvious respectively (Figures 8c,g), implies that the crystallization of minerals such as apatite and zircon was not significant (Wang et al., 2018).

Beyond fractional crystallization, partial melting in the mantle source also plays a crucial role in shaping the trace element characteristics of these samples. The La/Sm and Sm/Yb ratios are particularly informative for inferring the source characteristics and the degree of partial melting of mantle-derived samples (Aldanmaz et al., 2000). Melts derived from garnet- or spinel-bearing peridotite are expected to be enriched in LREE, with relatively depleted MREE. Heavy rare earth elements (HREE), such as Yb, are compatible with garnet but incompatible with other mantle phases (Mysen, 1979; Irving and Frey, 1984). As a result, HREE enrichment would occur if garnet were present in the source. In the spinel-bearing peridotite stable field, an increase in the degree of partial melting leads to a decrease in the La/Sm ratio of the melt, while the Sm/Yb ratio remains relatively constant. In contrast, within the garnet-bearing peridotite stability field, increasing partial melting results in a significant decrease in both the La/Sm and Sm/Yb ratios. Figure 7b illustrates this concept, comparing potential mantle sources, such as depleted MORB mantle (DMM), primary mantle (PM), and Kerguelen plume-derived magmas (sample s749C-16R-16 from Site 749, Frey et al., 2000). The simulation calculation of variations in REE ratios, as depicted in the La/Sm-Sm/Yb diagram (Figure 7b), suggests that samples display characteristics typical of ocean island basalts (OIB). These samples are plotted within the 5%–10% partial melting range of garnet peridotite in the primitive mantle (PM), implying that the mafic rocks in the Zhegu area primarily formed through low-degree partial melting of garnet-bearing peridotite.

5.2.3 Magmatic source

This study investigates the ratios of incompatible elements (Supplementary Table 3; Figure 9c) to characterize the trace element composition of the source region. The results suggest that the incompatible element ratios of the mafic rocks in the Zhegu area closely resemble those of the Sangxiu Formation basalt, Hawaiian basalt, Kerguelen OIB, Emeishan high-Ti basalt, and 90°E ridge

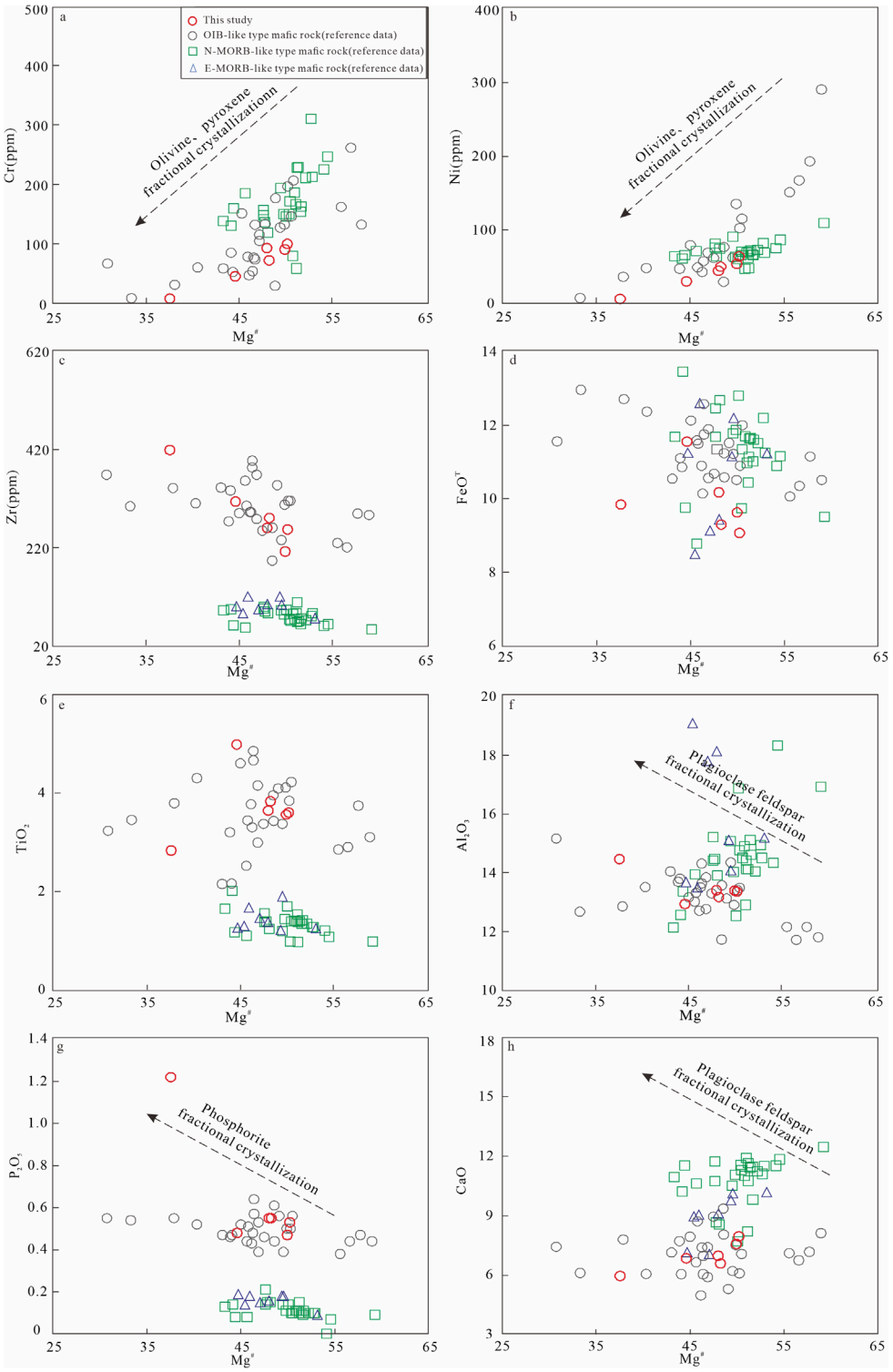

FIGURE 8
Correlations of selected major and trace elements vs. $Mg^{\#}$.

basalt. This resemblance suggests that the source of mafic rocks in the Zhegu region is analogous to that of hotspot or mantle plume magmas. In the OIB source discrimination diagram, all samples fall within or near the OIB field (Figure 9). Coupled with the similar geochemical, REE and trace element distribution patterns (Figure 5), this indicates that the mafic rocks in the Zhegu area

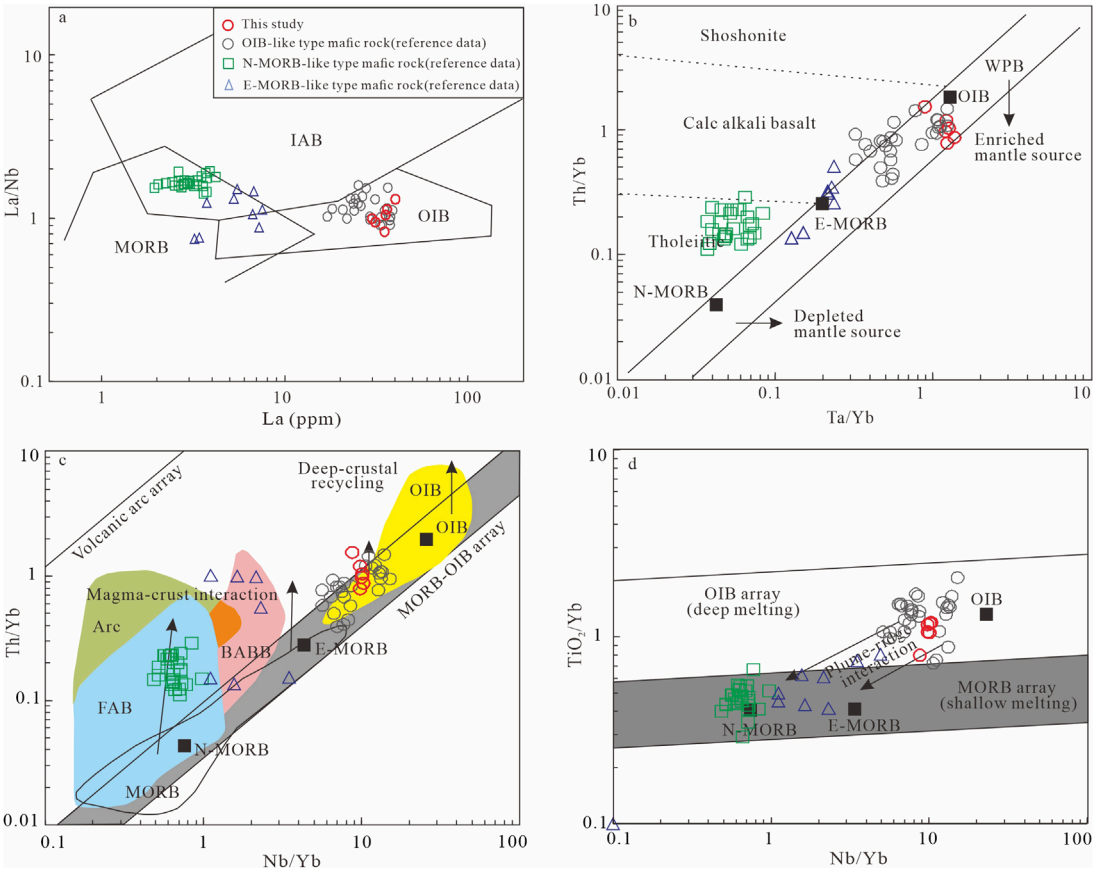

FIGURE 9
The La/Nb versus La **(a)** (after Li (1993)); Ta/Yb versus Th/Yb **(b)** (after Wilson (1989)); Nb/Yb versus Th/Yb **(c)** (after Pearce (2008)); Nb/Yb versus TiO_2/Yb **(d)** (after Pearce (2008)) diagrams of mafic dyke rocks from the Zhegu area in southern Tibet.

likely originate from a mantle source akin to OIB, potentially the product of hotspot or mantle plume activity (Zhu et al., 2005; Yang et al., 2015; Chen et al., 2018). Previous research indicates that mafic dykes originating from the depleted mantle should have a Zr/Nb ratio greater than 18 (Zheng et al., 2020). However, the Zr/Nb ratios of the Zhegu mafic rocks range from 6.95 to 13.5, all below 18. Additionally, in the Ta/Yb-Th/Yb diagram (Figure 9c), samples in the Zhegu area show an enriched mantle characteristic. In addition, the mafic rocks in the Zhegu area also have been influenced by lithospheric mantle materials. Firstly, the enrichment of LILE (such as Rb and Ba) in the mafic rocks of the Zhegu area suggests the involvement of the lithospheric mantle (Coffin and Eldholm, 1992). Secondly, the incompatible element ratios of the Zhegu mafic rocks are similar to those of the Sangxiu Formation basalts in Supplementary Table 3, which previous studies have attributed to the influence of the lithospheric mantle (Zhu et al., 2005).

In summary, we propose that the source of the Zhegu mafic rocks is similar to that of OIB-type mafic dyke swarms within the Tethys Himalayan tectonic belt of southern Tibet (Jiang et al., 2007; Qiu, 2011; Ren et al., 2014; Cheng et al., 2022). These rocks represent products of the interaction between enriched hotspots or mantle plume sources and the lithospheric mantle.

5.3 Tectonic setting

Mafic dyke swarms typically form as a result of the rapid intrusion of mafic magma from deep sources into the near-surface crust under conditions of crustal extension. These swarms can provide valuable insights into the geodynamic settings of the region.

The OIB are a prominent type of igneous rocks found within ocean basins and are considered a representative product of magmatic processes occurring in these regions. Similarly, in continental rifts, igneous rocks with geochemical characteristics similar to OIB can also develop. In addition to intraplate tectonic settings, OIB-like magmatic rocks can form in back-arc extensional rifts associated with subduction-related arc magmatism (Liu et al., 2017; Gao et al., 2018, 2021). However, since the Early Cretaceous OIB-like basalts in the Tethys Himalayan Belt are not contemporaneous with arc magmatism (Yang et al., 2022), we tend to exclude this possibility.

In the Zr-Zr/Y and Ta/Hf-Th/Hf diagrams (Figures 10a,b), all samples fall within the intraplate basalt region, aligning with previous studies (Zhu et al., 2004, 2005; Jiang et al., 2007; Ren et al., 2015), suggesting that these rocks formed in intraplate tectonic environments. Zhu et al. (2009a), Zhu et al. (2013) proposed that extensive magmatic activity during the Early Cretaceous in

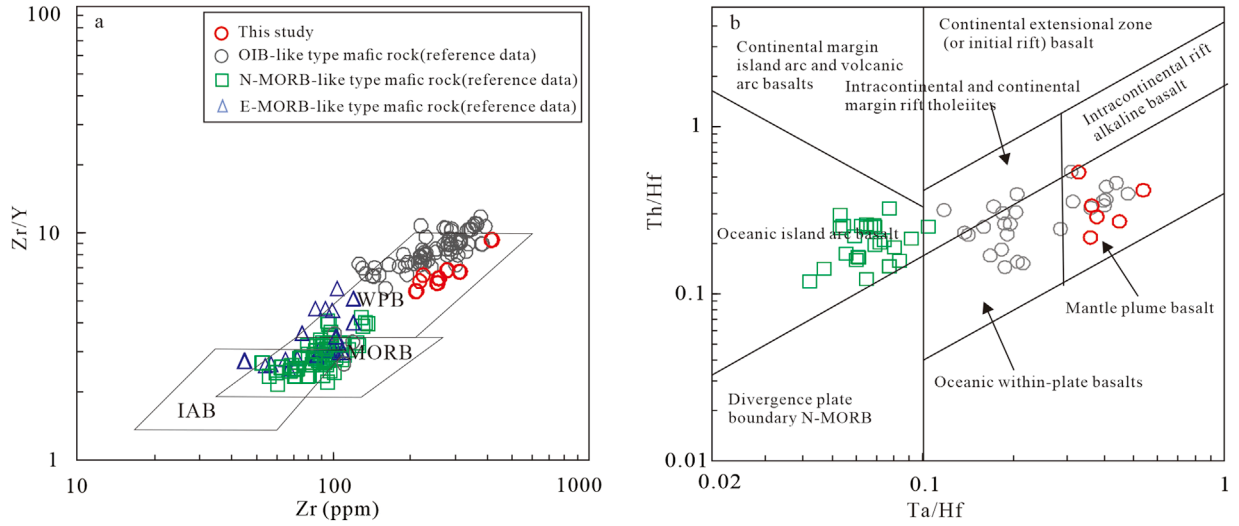

FIGURE 10
Zr/Y versus Zr **(a)** [after Pearce and Norry (1979)]; Th/Hf versus Ta/Hf **(b)** [after Wang et al. (2001)] diagrams of the mafic dyke rocks from the Zhegu area in southern Tibet.

the Comei LIP contributed to the formation of OIB-type mafic igneous rocks, which are distributed across regions such as Nagarze, Lhozhag, Cona, and Comei. Further research has indicated that the mantle plume head of the Comei LIP is compositionally similar to that of the Kerguelen mantle plume, suggesting a common magma source (Frey et al., 1996). Recent chronology and geochemical studies also support the hypothesis that the Early Cretaceous OIB-type basalts in the Tethys Himalayan Belt are closely related to early-stage activity of the Kerguelen Mantle plume (Zhu et al., 2005, 2008b; 2013; Qiu et al., 2010; Xia et al., 2012; Liu et al., 2015; Wang et al., 2016; Wei et al., 2017; Zhou et al., 2017; Tian et al., 2019). The OIB-type mafic rocks of the Comei LIP are characterized by high TiO_2 (average of ~3.0 wt.%) and P_2O_5 (average of ~0.4 wt.%) with no Nb-Ta negative anomalies (Xia et al., 2012). This study finds that the mafic rocks in the Zhegu area also exhibit TiO_2 (average of ~3.74 wt.%) and P_2O_5 (average of ~0.63 wt.%), and similarly lack negative Nb-Ta anomalies, resembling the characteristics of the mafic rocks in the Comei LIP. Additionally, the formation ages of diabase and gabbro (130.7 ± 1.5 Ma and 131.6 ± 2.5 Ma, respectively) in this study coincide with the age range of OIB-type rocks in the Comei LIP (130–136 Ma) (Zhu et al., 2009b), which are products of the early-stage activity of the Kerguelen mantle plume.

In conclusion, the mafic rocks in the Zhegu area are part of the Comei Large Igneous Province and likely represent products of early Kerguelen mantle plume activity.

6 Conclusion

(1) Zircon U-Pb dating indicates that diabase and gabbro crystallized during the Early Cretaceous period, with ages of 130.7 ± 1.5 Ma and 131.6 ± 2.5 Ma, respectively, which are comparable to the formation age of OIB-type mafic rocks found in the Comei Large Igneous Province. The trace elements distribution patterns of mafic igneous rocks in Zhegu area are similar with that of OIB.

(2) The mafic rocks in the Zhegu area experiences fractional crystallization. And the assimilation of crust materials was insignificant. They are products of the interaction between enriched hotspots/mantle plumes and the lithospheric mantle, which was associated with the early activity of the Kerguelen mantle plume.

Data availability statement

The original contributions presented in the study are included in the article/Supplementary Material, further inquiries can be directed to the corresponding authors.

Author contributions

MC: Data curation, Funding acquisition, Investigation, Project administration, Writing – original draft, Writing – review and editing. SS: Conceptualization, Funding acquisition, Project administration, Supervision, Writing – review and editing. YL: Formal Analysis, Funding acquisition, Methodology, Resources, Software, Writing – original draft. YM: Investigation, Methodology, Validation, Visualization, Writing – original draft. YT: Data curation, Investigation, Software, Validation, Writing – original draft. XL: Formal Analysis, Methodology, Resources, Visualization, Writing – original draft. MZ: Methodology, Resources, Software, Writing – original draft. XH: Formal Analysis, Funding acquisition, Project administration, Validation, Writing – original draft. TW: Investigation, Project administration, Software, Validation, Writing – original draft. HZ: Formal Analysis, Methodology, Validation, Visualization, Writing – original draft. KX: Formal Analysis, Resources, Validation,

Visualization, Writing – original draft. CC: Formal Analysis, Investigation, Methodology, Software, Writing – original draft. JZ: Data curation, Methodology, Supervision, Writing – review and editing. WG: Funding acquisition, Project administration, Supervision, Writing – original draft.

Funding

The author(s) declare that financial support was received for the research and/or publication of this article. This study was supported by the National Key R&D Program of China (2023YFF0807103), the National Natural Science Foundation of China (42373049), the China Geological Survey Project (1212011220659, DD20230527, ZD20220309, DD20243079), the Taishan Scholar Program of Shandong (tspd20230609) and Laoshan Laboratory (LSKJ202204100).

Conflict of interest

The authors declare that the research was conducted in the absence of any commercial or financial relationships that could be construed as a potential conflict of interest.

Generative AI statement

The author(s) declare that no Generative AI was used in the creation of this manuscript.

Publisher's note

Supplementary material

The Supplementary Material for this article can be found online at: https://www.frontiersin.org/articles/10.3389/feart.2025.1513583/full#supplementary-material

References

Aldanmaz, E., Pearce, J. A., Thirlwall, M. F., and Mitchell, J. G. (2000). Petrogenetic evolution of late Cenozoic, post-collision volcanism in western Anatolia, Turkey. *J. Volcanol. Geotherm. Res.* 102 (1), 67–95. doi:10.1016/S0377-0273(00)00182-7

Baksi, A. K. (1995). Petrogenesis and timing of volcanism in the Rajmahal flood basalt province, northeastern India. *Chem. Geol.* 121 (1), 73–90. doi:10.1016/0009-2541(94)00124-Q

Chen, S. S., Fan, W. M., Shi, R. D., Liu, X. H., and Zhou, X. J. (2018). 118–115 Ma magmatism in the Tethyan Himalaya igneous province: Constraints on early cretaceous rifting of the northern margin of greater India. *Earth Planet. Sci. Lett.* 491, 21–33. doi:10.1016/j.epsl.2018.03.034

Cheng, M., Hu, X., Tang, Y., Deng, Z., Min, Y., Chen, S., et al. (2024). Pan-African and early paleozoic orogenic events in southern Tibet: Evidence from geochronology and geochemistry of the Kangbuzhenri Gneissic granite in the Zhegu area. *Minerals* 14 (8), 845. doi:10.3390/min14080845

Cheng, M., Lou, Y. L., Tang, R., Liao, J., Chen, S. M., Li, Y., et al. (2022). Zircon U-Pb dating, geochemistry characteristics and tectonic implications of mafic dykes in the Chaiwa area, Southern Tibet. *Acta Petrologica Mineralogica* 41 (3), 504–518. doi:10.3969/j.issn.1000-6524.2022.03.002

Coffin, M., and Eldholm, O. (1992). Volcanism and continental break-up: A global compilation of large igneous provinces. *Geol. Soc.* 68. 17–30. doi:10.1144/GSL.SP.1992.068.01.02

Coffin, M. F., Pringle, M. S., Duncan, R. A., Gladczenko, T. P., Storey, M., Müller, R. D., et al. (2002). Kerguelen hotspot magma output since 130 Ma. *J. Petrol.* 43 (7), 1121–1137. doi:10.1093/petrology/43.7.1121

Condie, K. C., Frey, B. A., and Kerrich, R. (2002). The 1.75-Ga Iron King Volcanics in west-central Arizona: a remnant of an accreted oceanic plateau derived from a mantle plume with a deep depleted component. *Lithos* 64 (1), 49–62. doi:10.1016/S0024-4937(02)00158-5

Ding, F., Gao, J. G., and Xu, K. Z. (2020). Geochemistry, geochronology and geological significances of the basic dykes in Rongbu area, southern Tibet. *Acta Petrol. Sin.* 36 (2), 391–408. doi:10.18654/1000-0569/2020.02.04

Frey, F. A., Coffin, M. F., Wallace, P. J., Weis, D., Zhao, X., Wise, S. W., et al. (2000). Origin and evolution of a submarine large igneous province: the Kerguelen Plateau and Broken Ridge, southern Indian Ocean. *Earth Planet. Sci. Lett.* 176 (1), 73–89. doi:10.1016/S0012-821X(99)00315-5

Frey, F. A., Green, D. H., and Roy, S. D. (1978). Integrated models of basalt petrogenesis: A study of quartz Tholeiites to olivine melilitites from south Eastern Australia utilizing geochemical and experimental petrological data. *J. Petrology* 19 (3), 463–513. doi:10.1093/petrology/19.3.463

Frey, F. A., McNaughton, N. J., Nelson, D. R., deLaeter, J. R., and Duncan, R. A. (1996). Petrogenesis of the Bunbury Basalt, western Australia: interaction between the Kerguelen plume and Gondwana lithosphere? *Earth Planet. Sci. Lett.* 144 (1), 163–183. doi:10.1016/0012-821X(96)00150-1

Frey, F. A., Weis, D., Borisova, A. Y., and Xu, G. (2002). Involvement of continental crust in the formation of the cretaceous Kerguelen plateau: New perspectives from ODP leg 120 sites. *J. Petrology* 43 (7), 1207–1239. doi:10.1093/petrology/43.7.1207

Gao, X., Yu, S., Peng, Y., Lv, P., Wang, M., Liu, Y., et al. (2021). Insights into OIB-like magmatism contemporaneous with oceanic subduction: Petrogenetic constraints on the Kendelong metagabbro in the North Qaidam. *Lithos* 392-393, 106130. doi:10.1016/j.lithos.2021.106130

Gao, Z., Zhang, H. F., Yang, H., Pan, F. B., Luo, B. J., Guo, L., et al. (2018). Back-arc basin development: Constraints on geochronology and geochemistry of arc-like and OIB-like basalts in the Central Qilian block (Northwest China). *Lithos* 310-311, 255–268. doi:10.1016/j.lithos.2018.04.002

Hess, P. C. (1992). *Phase equilibria constraints on the origin of ocean floor basalts*, 71. Geophysical Monograph.

Hoskin, P. W. O., and Black, L. P. (2000). Metamorphic zircon formation by solid-state recrystallization of protolith igneous zircon. *J. Metamorph. Geol.* 18 (4), 423–439. doi:10.1046/j.1525-1314.2000.00266.x

Huang, Y., Liang, W., Zhang, L. K., Li, G. M., Huang, C. M., Xiao, X. B., et al. (2018). The initial break-up between Tethyan-Himalaya and Indian Terrane: evidences from Late Cretaceous OIB-type basalt in southern Tibet. *Earth Sci.* 43 (08), 2651–2663.

Irving, A. J., and Frey, F. A. (1984). Trace element abundances in megacrysts and their host basalts: Constraints on partition coefficients and megacryst genesis. *Geochimica Cosmochimica Acta* 48 (6), 1201–1221. doi:10.1016/0016-7037(84)90056-5

Jiang, S. H., Nie, F. J., Hu, P., and Liu, Y. (2010). An important spreading event of the neo-tethys ocean during the late Jurassic and early cretaceous: Evidence from Zircon U-Pb SHRIMP dating on diabase in Nagarzê, southern Tibet. *Acta Geol.* 80, 522–527. doi:10.1111/j.1755-6724.2006.tb00272.x

Jiang, S. H., Nie, F. J., Hu, P., Liu, Y., and Lai, X. R. (2007). Geochemical characteristics of the mafic dyke swarms in South Tibet. *Acta Geol. Sin.* 81 (01), 60–71. doi:10.3321/j.issn:0001-5717.2007.01.008

Kent, W., Saunders, A. D., Kempton, P. D., and Ghose, N. C. (1997). *Rajmahal basalts, eastern India: Mantle sources and melt distribution at a volcanic rifted margin*, 100. Washington DC American: Geophysical Union Geophysical Monograph.

Kinzler, R. J. (1997). Melting of mantle peridotite at pressures approaching the spinel to garnet transition: Application to mid-ocean ridge basalt petrogenesis. *J. Geophys. Res. Solid Earth* 102 (B1), 853–874. doi:10.1029/96JB00988

Lassiter, J. C., and DePaolo, D. J. (1997). Plume/Lithosphere Interaction in the generation of continental and oceanic flood basalts: chemical and isotopic constraints. *Large Igneous*.

Li, S. G. (1993). Ba-Nb-Th-La diagrams used to identify tectonic enviroments of ophiolite. *Acta Petrol. Sin.* (02), 146–157.

Li, Y., Ding, F., Yang, L., Xie, X., Xu, K., Li, Q., et al. (2019). Geochemical characteristics and geological significance of basalts in the Sangxiu formation, Rongbu area, southern Tibet. *Arabian J. Geosciences* 12 (24), 757. doi:10.1007/s12517-019-4880-4

Liang, F. H., Xu, Z. Q., Ba, D. Z., Xu, X. Z., Liu, F., and Xiong, F. H. (2011). Tectonic occurrence and emplacement mechanism of ophiolites from Luobusha-Zedang, Tibet. *Acta Petrol. Sin.* 27 (11), 3255–3268.

Lin, B., Tang, J., Chen, Y., Baker, M., Song, Y., Yang, H., et al. (2019). Geology and geochronology of Naruo large porphyry-breccia Cu deposit in the Duolong district, Tibet. *Gondwana Res.* 66, 168–182. doi:10.1016/j.gr.2018.07.009

Liu, D. Y., Jian, P., Zhang, Q., Zhang, F. Q., Shi, Y. R., Shi, G. H., et al. (2003). SHRIMP dating of adakites in the tulingkai ophiolite, Innr Mongolia: evidence for the early paleozoic subduction. *Acta Geol. Sin.* (03), 317–327. doi:10.3321/j.issn:0001-5717.2003.03.004

Liu, F., Yang, J. S., Chen, S. Y., Li, Z. L., Lian, D. Y., Zhou, W. D., et al. (2015). Geochemistry and Sr-Nd-Pb isotopic composition of mafic rocks in the western part of Yarlung Zangbo suture zone: Evidence for intra-oceanic supra-subduction within the Neo-Tethys. *Geol. China* 36 (04), 441–454. doi:10.3969/j.issn.1000-3657.2013.03.007

Liu, H., Wang, Y., Cawood, P. A., and Guo, X. (2017). Episodic slab rollback and back-arc extension in the Yunnan-Burma region: Insights from Cretaceous Nb-enriched and oceanic-island basalt–like mafic rocks. *GSA Bull.* 129 (5-6), 698–714. doi:10.1130/B31604.1

Liu, Z., Zhou, Q., Lai, Y., Qing, C., Li, Y., Wu, J., et al. (2015). Petrogenesis of the early cretaceous Laguila bimodal intrusive rocks from the Tethyan Himalaya: Implications for the break-up of eastern Gondwana. *Lithos* 236-237, 190–202. doi:10.1016/j.lithos.2015.09.006

Mahoney, J. J., Jones, W. B., Frey, F. A., Salters, V. J. M., Pyle, D. G., and Davies, H. L. (1995). Geochemical characteristics of lavas from Broken ridge, the naturaliste plateau and southernmost Kerguelen plateau: Cretaceous plateau volcanism in the southeast Indian ocean. *Chem. Geol.* 120 (3), 315–345. doi:10.1016/0009-2541(94)00144-W

McDonough, W. F. (1990). Constraints on the composition of the continental lithospheric mantle. *Earth Planet. Sci. Lett.* 101 (1), 1–18. doi:10.1016/0012-821X(90)90119-I

McKenzie, D., and O'Nions, R. K. (1991). Partial melt distributions from Inversion of rare earth element concentrations. *J. Petrology* 32 (5), 1021–1091. doi:10.1093/petrology/32.5.1021

Middlemost, E. A. K. (1994). Naming materials in the magma/igneous rock system. *Earth-Science Rev.* 37 (3), 215–224. doi:10.1016/0012-8252(94)90029-9

Miyashiro, A. (1974). Volcanic rock series in island arcs and active continental margins. *Am. J. Sci.* 274 (4), 321–355. doi:10.2475/ajs.274.4.321

Mysen, B. O. (1979). Trace-element partitioning between garnet peridotite minerals and water-rich vapor; experimental data from 5 to 30 kbar. *Am. Mineralogist* 64 (3-4), 274–287.

Neal, C. R., Mahoney, J. J., and Chazey, W. J. (2002). Mantle sources and the highly variable role of continental lithosphere in basalt petrogenesis of the Kerguelen plateau and Broken ridge LIP: Results from ODP leg 183. *J. Petrology* 43 (7), 1177–1205. doi:10.1093/petrology/43.7.1177

Pan, G. T., Wang, L. Q., and Zhu, D. C. (2004). Thoughts on some important scientific problems in regional geological survey of the Qinghai-Tibet Plateau. *Geol. Bull. China* 23 (01), 12–19.

Pearce, J. A. (1982). Trace element characteristics of lavas from destructive plate boundaries.

Pearce, J. A. (2008). Geochemical fingerprinting of oceanic basalts with applications to ophiolite classification and the search for Archean oceanic crust. *Lithos* 100 (1), 14–48. doi:10.1016/j.lithos.2007.06.016

Pearce, J. A., and Norry, M. J. (1979). Petrogenetic implications of Ti, Zr, Y, and Nb variations in volcanic rocks. *Contributions Mineralogy Petrology* 69 (1), 33–47. doi:10.1007/BF00375192

Qiu, B. B. (2011). The westward extension of Comei fragmented large igneous province in southem Tibet and its implications. *Acta Petrol. Sin.* 26 (7), 2207–2216.

Qiu, B. B., Zhu, D. C., Zhao, Z. D., and Wang, L. Q. (2010). The westward extension of Comei fragmented large igneous province in southern Tibet and its implications. *Acta petrol. Sin.* 26 (07), 2207–2216.

Ren, C., Liu, S., Zhu, L. D., Pan, J. T., and Gao, W. X. (2014). Geochemistry and Zircon SHRIMP U-Pb dating and their tectonic significance for intermediate-basic dyke in the Gudui region, South Tibet. *J. Sichuan Geol.* 34 (04), 496–500.

Ren, C., Ma, F. Z., Zhu, Z. H., Zhang, J. G., Huang, R. C., and Zhang, Y. (2015). U-Pb SHRIMP zircon ages of the mafic-ultramafic rocks from Chigu Co of South Tibet and their geological significances. *Geol. China* 42 (4), 881–890.

Rudnick, R., and Gao, S. (2003). Composition of the continental crust. *Treatise geochem.* 3, 1–64. doi:10.1016/B0-08-043751-6/03016-4

Shaw, D. M. (1970). Trace element fractionation during anatexis. *Geochimica Cosmochimica Acta* 34 (2), 237–243. doi:10.1016/0016-7037(70)90009-8

Sun, S. J., Ireland, T. R., Zhang, L., Zhang, R., Zhang, C., and Sun, W. (2018). Palaeoarchaean materials in the Tibetan Plateau indicated by zircon. *Int. Geol. Rev.* 60 (8), 1061–1072. doi:10.1080/00206814.2017.1367967

Sun, S. S., and McDonough, W. (1989). *Chemical and isotopic systematics of oceanic basalts: implications for mantle composition and processes*, 42. London: Special Publications, 313–345.

Taylor, S. R., and McLennan, S. M. (1985). *The continental crust: Its composition and evolution*. Oxford: Blackwell Scientific Publications, 312pp.

Thompson, R. N., Morrison, M. A., Dickin, A. P., and Hendry, G. L. (1984). *An assessment of the relative roles of crust and mantle in magma genesis: an elemental approach*, 310, 549–590.

Tian, Y., Gong, J., Chen, H., Guo, L., Xu, Q., Chen, L., et al. (2019). Early Cretaceous bimodal magmatism in the eastern Tethyan Himalayas, Tibet: Indicative of records on precursory continental rifting and initial breakup of eastern Gondwana. *Lithos* 324-325, 699–715. doi:10.1016/j.lithos.2018.12.001

Tong, J. S., Liu, J., Zhong, H. M., Xia, J., and Li, Y. H. (2007). Zircon U- Pb dating and geochemistry of mafic dike swarms in the Lhozag area, southern Tibet, China, and their tectonic implications. *Geol. Bull. China* 26 (12), 1654–1664.

Walter, M. J. (1998). Melting of garnet peridotite and the origin of komatiite and depleted lithosphere. *J. Petrology* 39, 29–60. doi:10.1093/petrology/39.1.29

Wang, X. C., Xia, B., Liu, W. L., Zhong, Y., Hu, X. C., Guan, Y., et al. (2018). Geochronology, geochemistry and petrogenesis of the Pungco Ophiolite, Tibet. *Geotect. Metallogenia* 42 (03), 550–569. doi:10.16539/j.ddgzyckx.2018.03.010

Wang, Y., Zeng, L., Hou, K., Gao, L. E., Wang, Q., Zhao, L., et al. (2022). Mantle source components and magmatic evolution for the Comei large igneous province: Evidence from the early cretaceous Niangzhong mafic magmatism in Tethyan Himalaya. *J. Earth Sci.* 33 (1), 133–149. doi:10.1007/s12583-021-1464-5

Wang, Y. L., Zhang, C. J., and Xiu, S. Z. (2001). Th/Hf-Ta/Hf idenfication of tectonic setting of basalts. *Acta Petrol. Sin.* 17, 413–421.

Wang, Y. Y., Gao, L. E., Zeng, L. S., Chen, F. K., Hou, K. J., Wang, Q., et al. (2016). Multiple phases of cretaceous mafic magmatism in the Gyangze-Kangma area, Tethyan Himalaya, southern Tibet. *Acta Petrol. Sin.* 32 (12), 3572–3596.

Wang, Y. Y., Zeng, L. S., Gao, L. E., Zhao, L. H., and Yan, L. L. (2024). Early arrival of the Reunion plume at the base of the Himalaya? *Earth Planet. Sci. Lett.* 639, 118756. doi:10.1016/j.epsl.2024.118756

Wei, Y., Liang, W., Shang, Y., Zhang, B., and Pan, W. (2017). Petrogenesis and tectonic implications of ~130Ma diabase dikes in the western Tethyan Himalaya (western Tibet). *J. Asian Earth Sci.* 143, 236–248. doi:10.1016/j.jseaes.2017.04.008

Wilson, M. (1989). *Igneous petrogenesis*. London: Unwin Hyman.

Workman, R. K., and Hart, S. R. (2005). Major and trace element composition of the depleted MORB mantle (DMM). *Earth Planet. Sci. Lett.* 231 (1), 53–72. doi:10.1016/j.epsl.2004.12.005

Xia, Y., Zhu, D. C., Zhao, Z. D., Wang, Q., Yuan, S. H., Chen, Y., et al. (2012). Whole-rock geochemistry and zircon Hf isotope of the OIB-type mafic rocks from the Comei Large Igneous Province in southeastern Tibet. *Acta Petrol. Sin.* 28 (5), 1588–1602.

Yang, C. Y., Li, Y. B., Zhang, J. S., and Zhang, G. (2022). Geochronology, petrogenesis and tectonic significance of the Kalong gabbro from Nagarze, South Tibet. *Chin. J. Geol.* 57 (02), 399–414.

Yang, G., Li, Y., Xiao, W., and Tong, L. (2015). OIB-type rocks within West Junggar ophiolitic mélanges: Evidence for the accretion of seamounts. *Earth-Science Rev.* 150, 477–496. doi:10.1016/j.earscirev.2015.09.002

Yin, A. (2006). Cenozoic tectonic evolution of the Himalayan orogen as constrained by along-strike variation of structural geometry, exhumation history, and foreland sedimentation. *Earth-Science Rev.* 76 (1), 1–131. doi:10.1016/j.earscirev.2005.05.004

Yu, G. M., and Wang, C. S. (1990). *Tibet titis Deposition geology*. Beijing: Beijing Geological Publishing House.

Yu, Y. Z., and Liu, Z. C. (2023). Origin and genetic mechanism of the early cretaceous metabasite from the Ramba area, Tethyan Himalaya geological. *J. China Univ.* 29 (04), 527–542.

Zhang, Y. X., Xie, C. M., Yu, Y. P., Zhang, H. Y., and Dong, Y. C. (2018). The Early Jurassic subduction of Neo-Tethyan oceanic slab: Constraints from zircon U-Pb age and Hf isotopic compositions of Sumdo high-Mg diorite. *Geol. Bull. China* 37 (08), 1387–1399.

Zhang, Z. C., Wang, F. S., Hao, Y. L., and Mahoney, J. J. (2004). Geochemistry of the Picrites and associated basalts from the Emeishan large igneous basalt province and constraints on their source region. *Acta Geol. Sin.* (02), 171–180. doi:10.3321/j.issn:0001-5717.2004.02.005

Zheng, J. L., Liu, T., Xu, L. M., Liang, Z. K., Guo, X. Y., Wang, D. K., et al. (2020). Geochemical and chronologic characteristics of ultramafic rocks in Gaxian ophiolitic

mélange of the Da Hinggan Mountains and their geological significance. *Geol. Bull. China* 39 (4), 480–490.

Zhong, H. M., Tong, J. S., Xia, J., Lu, R. K., and Qiu, J. Q. (2005). Characteristics and tectonic setting of volcanic rocks of the Sangxiu Formation in the southern part of Yamzho Yumco, southern Tibet. *Geol. Bull. China* 24 (1), 72–79.

Zhou, Q., Liu, Z., Lai, Y., Wang, G. C., Liao, Z. W., Li, Y. X., et al. (2017). Petrogenesis of mafic and felsic rocks from the Comei large igneous province, South Tibet: Implications for the initial activity of the Kerguelen plume. *GSA Bull.* 130 (5-6), 811–824. doi:10.1130/B31653.1

Zhu, D. C., Chung, S. L., Mo, X. X., Zhao, Z. D., Niu, Y., Song, B., et al. (2009a). The 132 Ma Comei-Bunbury large igneous province: Remnants identified in present-day southeastern Tibet and southwestern Australia. *Geology* 37 (7), 583–586. doi:10.1130/G30001A.1

Zhu, D. C., Mo, X. X., Pan, G. T., Zhao, Z. D., Dong, G. C., Shi, Y. R., et al. (2008b). Petrogenesis of the earliest Early Cretaceous mafic rocks from the Cona area of the eastern Tethyan Himalaya in south Tibet: Interaction between the incubating Kerguelen plume and the eastern Greater India lithosphere? *Lithos* 100 (1), 147–173. doi:10.1016/j.lithos.2007.06.024

Zhu, D. C., Mo, X. X., Zhao, Z. D., Niu, Y. L., and Chung, S. L. (2008a). Whole-rock elemental and zircon Hf isotopic geochemistry of mafic and ultramafic rocks from the Early Cretaceous Comei large igneous province in SE Tibet: constraints on mantle source characteristics and petrogenesis. *Himal. J. Sci.* 5, 178–180. doi:10.3126/hjs.v5i7.1350

Zhu, D. C., Mo, X. X., Zhao, Z. D., Niu, Y. L., Pan, G. T., Wang, L. T., et al. (2009b). Permian and early cretaceous tectonomagmatism in southern Tibet and Tethyan evolution: New perspective. *Earth Sci. Front.* 16 (2), 001–020.

Zhu, D. C., Pan, G. T., Mo, X. X., Liao, Z. L., Jiang, X. S., Wang, L. Q., et al. (2005). Geochemistry and petrogenesis of the Sangxiu Formation basalts in the central segment of Tethyan Himalaya. *Geochim. (01)*, 7–19.

Zhu, D. C., Pan, G. T., Mo, X. X., Liao, Z. L., Jiang, X. S., Wang, L. Q., et al. (2007). Petrogenesis of volcanic rocks in the Sangxiu Formation, central segment of Tethyan Himalaya: A probable example of plume–lithosphere interaction. *J. Asian Earth Sci.* 29 (2), 320–335. doi:10.1016/j.jseaes.2005.12.004

Zhu, D. C., Wang, L. Q., Pan, G. T., Mo, X. X., Liao, Z. L., Jiang, X. S., et al. (2004). Discrimination of OIB-type magma and its significances of basalts from middle Jurassic Zhela Formation in the central belt of Tethyan Himalayas, South Tibet. *Geol. Sci. Technol. Intell.* 23 (03), 15–24. doi:10.3969/j.issn.1000-7849.2004.03.004

Zhu, D. C., Xia, Y., Qiu, B. B., Wang, Q., and Zhao, Z. D. (2013). Why do we need to propose the Early Cretaceous Comei large igneous province in southeastern Tibet? *Acta Petrol. Sin.* 29 (11), 3659–3670.